Heteropolyacid-Encapsulated Self-Assembled Materials for Anhydrous Proton-Conducting Electrolytes

Masanori Yamada[†] and Itaru Honma*

Energy Technology Research Institute, National Institute of Advanced Industrial Science and Technology (AIST), 1-1-1 Umezono, Tsukuba, Ibaraki 305-8568, Japan

Received: June 6, 2006; In Final Form: July 26, 2006

The composite material of heteropolyacid (12-phosphotungstic acid; PWA) and polystyrene sulfonic acid (PSS) construct the PWA-encapsulated material by the self-assembly of $-SO_3H$ onto the PWA surface; as a result, the fast proton transfer occurred at the interface between the PWA and $-SO_3H$, and the encapsulated material indicated the high anhydrous proton conductivity of 1×10^{-2} S cm^{-1} at 180 °C. These anhydrous proton-conducting materials without the existence of water molecules are quite different from customary ion-exchange membrane, such as Nafion, and may have advantages as an electrolyte membrane for polymer electrolyte membrane fuel cells operating at intermediate temperatures under anhydrous conditions but also for electrochemical devices including electrochromic displays, chemical sensors, and others.

Introduction

$H_3PW_{12}O_{40}$ (12-phosphotungstic acid; PWA), one of the Keggin-type heteropolyacids, is considered to have a strong Brønsted acidity at the border between strong acids and superstrong acids.[1] Its primary structure is characterized by units ("Keggin") in which a central phosphorus atom in a tetrahedral coordination is surrounded by 12 edge-sharing metal−oxygen octahedra (WO_6). The negative charge of this structure is neutralized in the acidic form by three protons. These heteropolyacids are efficient catalysts for the selective oxidation of alkanes, aldehydes, and perfluorinated acids.[1−3] Additionally, heteropolyacids have been known to show a high proton conductivity under high humidity conditions.[4] Therefore, the hybrid materials consisting of organic polymers and heteropolyacids have been attracting attention for their use in polymer electrolyte membrane fuel cells (PEFC).[5,6] However, their protonic conductivity is highly sensitive to humidity and temperature, which limits their fuel cell applications. Especially, at high temperatures (>100 °C), the proton conductivity of PWA decreased by the evaporation of hydration water. Therefore, the proton conductive property or application of PWA at high temperature and anhydrous (water-free) conditions has not yet been reported. The anhydrous proton-conducting PWA material may have a potential not only for PEFC operating at high temperatures under anhydrous conditions but also for solid-state electrochemical devices including electrochromic displays, chemical sensors, and others.

The proton transport under anhydrous conditions might be based on a nonvehicular mechanism (Grotthuss mechanism), in which only protons are mobile from site to site without the assistance of diffusible vehicle molecules, such as water molecules.[7,8] The activation energy of this type of proton transport can primarily depend on the distance between the hopping sites. Therefore, acid−base composite materials have been the primary focus for the anhydrous proton conductive materials.[9] In this case, the acidic and basic molecules (polymers) act as proton donors and acceptors during the proton-transfer reactions, respectively. Namely, the proton transfer is controlled by the ΔpK_a value. Therefore, a similar transfer reaction might occur at not only the acid−base composite but also the acid−acid composite materials, which are composed of acidic and strong-acidic molecules, such as heteropolyacids. Therefore, we propose a novel proton-conducting structure and mechanism consisting of PWA and polystyrene sulfonic acid (PSS). Surprisingly, this material formed the PWA-encapsulated structure by the self-assembly of $-SO_3H$ onto the PWA surface and had the high anhydrous proton conductivity of 1×10^{-2} S cm^{-1} at 180 °C. Additionally, test using a nonhumidified H_2/O_2 fuel cell demonstrated power generation at 160 °C.

Experimental Section

Materials. PWA and PSS ($MW = 7 \times 10^4$, 30% solution in water) were obtained from Wako Pure Chemical Industries Ltd., Osaka, Japan, and Polysciences, Inc., PA, respectively. PWA-PSS composite materials were prepared as follows: PWA molecule was dissolved in pure water (100 mg mL^{-1}), and this PWA solution was added in PSS solution and stirred for 12 h at room temperature. This PWA-PSS mixed solutions were cast onto the Teflon plate, dried for 24 h at 70 °C, and then stripped from the plate. The mixing ratio was controlled by the additional amount of PWA solution.

Characterization of Composite Materials. The thermal stability of these composite materials was analyzed by thermogravimetric differential thermal analysis (TG-DTA) (TG-DTA 2000S, Mac Sciences Co., Ltd., Yokohama, Japan). TG-DTA measurement was performed at the heating rate of 10 °C min^{-1} under dry nitrogen flow. Infrared (IR) spectra of composite materials were characterized using an IR spectrophotometer FT/IR-6200 (JASCO Corporation, Tokyo, Japan). The IR spectrum was measured with the resolution of 4 cm^{-1}. The ^{1}H and ^{31}P magic-angle-spinning (MAS) NMR spectra were obtained using a Bruker MSL-400 spectrometer (Bruker BioSpin GmbH, Rheinstetten, Germany) or Chemagnetics CMX-300 (Varian,

* To whom correspondence should be addressed. Tel: +81 29 861 5648. Fax: +81 29 861 5799. E-mail: i.homma@aist.go.jp.
[†] Present Address: Okayama University of Science.

10.1021/jp063488k CCC: $33.50
Published on Web 09/26/2006

Figure 1. Photographs of PSS 10 wt % PWA composite material with thickness of ca. 500 μm.

Inc., Palo Alto, CA) spectrometer at the resonance frequencies of 400.13 and 121.533 MHz, respectively.

Conductivity Measurements. Proton conductivity of PWA-encapsulated material was demonstrated by the alternating current (AC) impedance method in a frequency range from 1 Hz to 1 MHz using an impedance analyzer SI-1260 (Solartron Co., Hampshire, UK) in a stainless vessel from room temperature to 180 °C. The PWA-encapsulated membrane sandwiched between two platinum electrodes (diameter: 6 mm) with the Teflon spacer. The direction of conductive measurement is perpendicular to the composite material. Conductivities of PWA-encapsulated materials were determined from a typical impedance response (Cole−Cole plots). The resistances of the composite materials were obtained from the extrapolation to the real axis. All the measurements in this experiment were carried out under dry nitrogen flow.

Performance Evaluation in Fuel Cell. The membrane electrode assembly (MEA) was prepared as follows: PWA-PSS solution was cast onto the silica filter (Advantec Toyo Kaisha, Ltd. Tokyo, Japan) to form a robust membrane and E-TEK Pt/C electrode with Pt loading 20 wt % (E-TEK Division of De Nora N.A., Inc., NJ) was put on the membrane. These MEAs were dried at 70 °C for 1−3 days. The dried MEA was subjected into the electrochemical cell chamber. All the fuel cell measurements were executed under flowing of dry H_2/O_2 at 0.1 MPa, H_2 100 mL min^{-1}, and O_2 100 mL min^{-1}. Current−voltage ($I-V$) characteristics of MEA were measured under anhydrous conditions. The flow rates of the gases were controlled using mass-flow controllers.

Results and Discussion

The PWA-PSS mixed solution was cast onto a plate and dried. The dried PWA-PSS composite material was stripped from the plate. Figure 1 shows the photograph of PSS 10 wt % PWA composite material. The thickness of membranes is ca. 500 μm. This brown free-standing membrane is transparent and homogeneous. Parts a and b of Figure 2 show the TG-DTA of (1) pure PSS, (2) PSS 10 wt % PWA, (3) PSS 30 wt % PWA, and (4) PSS 50 wt % PWA, respectively. This material showed a TG weight loss due to thermal decomposition above 180 °C. Additionally, at <180 °C, these materials did not show any DTA peaks except for the endothermic peak which was due to the evaporation of hydration water from the membrane. Therefore, the PWA-PSS composite material is a thermo-stable membrane (<180 °C). The large TG weight loss of PSS-PWA composite material above 200 °C is due to the thermal decomposition.

The molecular structures of PWA-PSS composite material, which was dried at 150 °C for 6 h, are characterized by the infrared (IR) spectroscopic analysis. Figure 3 shows the IR spectra of the PWA-PSS composite material of (a) pure PSS, (b) PSS 5 wt % PWA, (c) PSS 10 wt % PWA, (d) PSS 15 wt % PWA, (e) PSS 30 wt % PWA, (f) PSS 50 wt % PWA, and (g) pure PWA materials, respectively. Pure PWA showed

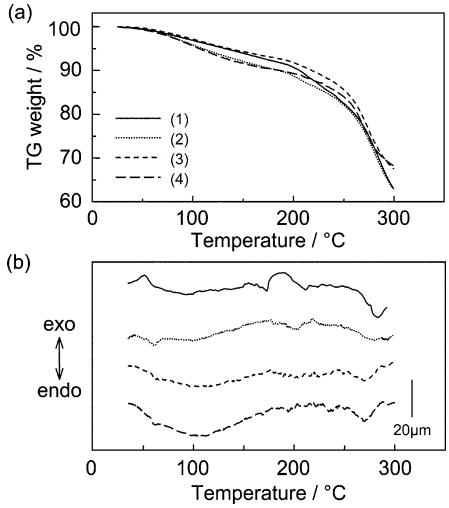

Figure 2. (a) TG and (b) DTA curves of PSS-PWA composite materials with the heating rate of 10 °C min^{-1} under dry nitrogen flow. (1) Pure PSS, (2) PSS 10 wt % PWA, (3) PSS 30 wt % PWA, and (4) PSS 50 wt % PWA.

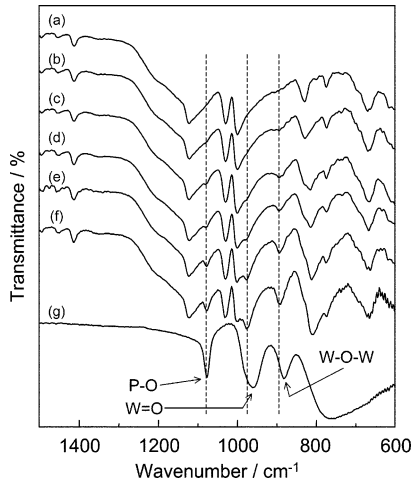

Figure 3. IR spectra of PWA-PSS composite materials with different mixing ratios of PWA: (a) pure PSS, (b) PSS 5 wt % PWA, (c) PSS 10 wt % PWA, (d) PSS 15 wt % PWA, (e) PSS 30 wt % PWA, (f) PSS 50 wt % PWA, and (g) pure PWA materials.

absorption bands at 950 and 875 cm^{-1}, attributed to the stretching vibration of the terminal oxygen, W═O, and bridging oxygen, W−O−W, respectively.[10] These absorption bands shifted by 15−25 cm^{-1} to a higher frequency by mixing of the PSS molecules (see the dashed line). These shifts might be due to the interaction through the hydrogen bonding between the W═O or W−O−W groups in the PWA molecules and the −SO_3H in the PSS molecules. Therefore, in the PWA-PSS composite material, PWA and −SO_3H may act as Brønsted acidic and basic molecules, respectively. In contrast, a frequency shift of the central tetrahedron P−O band at 1076 cm^{-1} [10] was not observed.

Next, we demonstrated the proton conductivity of the PWA-PSS composite material using the AC impedance method over the frequency range from 1 Hz to 1 MHz under dry nitrogen flow. Figure 4 shows the typical impedance response (Cole−Cole plots) of PSS 12.5 wt % PWA composite material at (□) 25 °C and (△) 90 °C under anhydrous conditions. The insert indicated the high-frequency range (100 Hz to 1 MHz) of PSS 12.5 wt % PWA composite material at (△) 90 °C and (○) 180 °C. Under a low conductivity (25 °C) situation, the Cole−Cole plots showed the semicircle component at high frequencies.

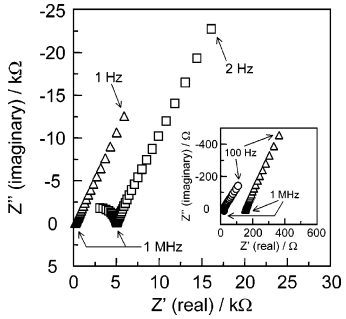

Figure 4. Typical impedance response (Cole−Cole plots) of PSS 10 wt % PWA composite materials at (□) 25 °C, (△) 90 °C, and (○) 180 °C. Frequency range is from 1 or 2 Hz to 1 MHz. The insert indicated the high-frequency range (1 kHz to 1 MHz) of PSS 10 wt % PWA composite materials.

However, this component has decreased with the increase of membrane's conductivity (see the plots obtained at 90 and 180 °C). Therefore, the resistances of the composite materials can be estimated from the intersection of the real axis and the linear part of the impedance spectra. These features of the Cole−Cole plots are similar to that of a highly ionic conducting membrane, such as humidified Nafion, an organic/inorganic hybrid membrane mixed with PWA,[5] or anhydrous proton conductors.[11−13] In contrast, these materials did not indicate the electronic conductivity under the direct current condition. Additionally, the diffusible ions other than protons do not exist in the composite materials (see the TG-DTA analyses in Figure 2). So, the impedance responses of the PWA-PSS composite material are due to the pure anhydrous proton transfer.[12−14] The PWA-PSS composite material in a stainless vessel was heated at 150 °C for 24 h under dry nitrogen flow. The proton conductivity slightly decreased with the increased heating time and reached a steady state at 15 h. Afterward, the materials were cooled to room temperature under dry nitrogen flow and then heated to measure the conductivity again. The steady-state anhydrous proton conductivity of (■) pure PSS, (□) PSS 5 wt % PWA, (●) PSS 10 wt % PWA, (○) PSS 12.5 wt % PWA, (▲) PSS 15 wt % PWA, (△) PSS 20 wt % PWA, (◆) PSS 30 wt % PWA, and (◇) PSS 50 wt % PWA materials in the temperatures range from room temperature to 180 °C are shown in Figure 5a. Figure 5b is the Arrhenius plot of the proton conductivity. The solid lines are the results of the least-squares fitting. The anhydrous proton conductivity increased with the temperature and reached a maximum value at 180 °C. The insert in Figure 5a indicated the anhydrous proton conductivity at 180 °C as a function of the PWA mixing ratios (wt %). Although the pure PWA material could not give measurable proton conductivity ($<10^{-8}$ S cm^{-1} at 160 °C) under anhydrous conditions, that of the PWA-PSS composite material increased with the doping of the PWA molecule and indicated the maximum proton conductivity of 1×10^{-2} S cm^{-1} at 10 wt % PWA. This conductivity is an extremely high value at 180 °C under anhydrous conditions. In contrast, the activation energy of the proton conduction was estimated from the slope of the Arrhenius plot. These energies were ca. 0.4 eV. This activation energy is one order higher than that of the customary humidified perfluorosulfonated electrolyte membrane[14] and almost the same as other materials, such as solid electrolytes,[7,15,16] fullerene derivatives,[17] and our composite materials for anhydrous proton conductors.[11−13] Additionally, PSS-PWA composite materials do not contain the free water by the heating at 150 °C for 24 h under dry nitrogen flow. Therefore, the proton transfer is considered to be based on a nonvehicular mechanism, in which only protons are mobile from site to site without the assistance

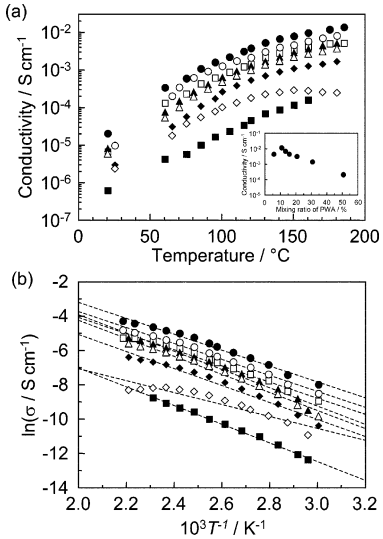

Figure 5. (a) Steady-state proton conductivities of PWA-PSS composite materials with different PWA mixing ratios under anhydrous conditions. The insert indicates the anhydrous proton conductivity at 180 °C as a function of the PWA mixing ratios. (b) Arrhenius plots of the proton conductivity of PWA-PSS composite materials. The solid lines are the results of the least-squares fitting. (■) pure PSS; (□) PSS 5 wt % PWA; (●) PSS 10 wt % PWA; (○) PSS 12.5 wt % PWA; (▲) PSS 15 wt % PWA; (△) PSS 20 wt % PWA; (◆) PSS 30 wt % PWA; (◇) PSS 50 wt % PWA materials.

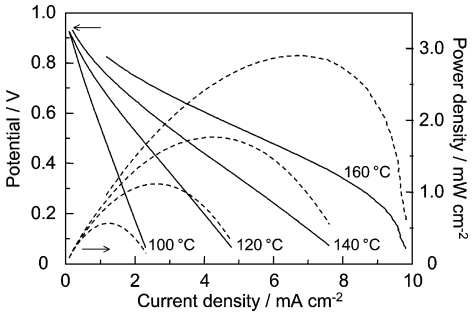

Figure 6. Cell voltage and power density vs current density of the fuel cell with PSS 10 wt % PWA composite electrolytes and E-TEK Pt/C electrode (Pt loading 20 wt %) at various cell temperatures under nonhumidified conditions.

of diffusible vehicle molecules, such as H_3O^+ or $H_5O_2^+$. Namely, these results suggest that the PWA-PSS composite are anhydrous proton-conducting materials.

Additionally, we demonstrated the fuel cell test of the PSS 10 wt % PWA MEA to confirm the proton transfer in the membrane under anhydrous conditions (nonhumidified H_2/O_2) (Figure 6). As a result, the current density and power density increased with the heating of the cell chamber and indicated the highest value at 160 °C. The maximum power density of approximately 3 mW cm^{-2} was obtained at the current density of 7 mA cm^{-2} and the cell voltage of 0.45 V. Additionally, the open circuit voltage (OCV) of 0.9−1.0 V is the conventional potential for the H_2/O_2 cell, and it indicates a very small gas permeability through the membrane. These results suggested free proton transfers in the PWA-PSS composite material at high temperatures under anhydrous conditions. However, the power outputs of the MEA cell under anhydrous conditions were lower than that expected from the proton conductivity value. This might be due to the high interfacial resistance between the membrane and E-TEK Pt/C electrode, because we did not optimize the interfacial resistance in the present work. Therefore, by improving this factor, the further power generation under anhydrous conditions might be expected.

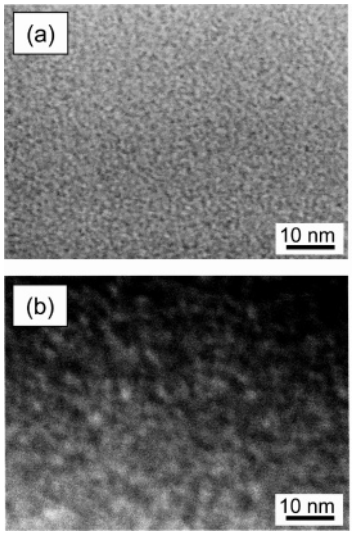

Figure 7. STEM images of PSS 10 wt % PWA composite material. (a) BF and (b) HAADF imaging modes.

Next, we performed the scanning transmission electron microscopy (STEM) and MAS NMR measurements of the PWA-PSS composite material to clarify its fast proton-conducting structure and mechanism. Parts a and b of Figure 7 show the STEM bright field (BF) and high-angle annular dark-field (HAADF) imaging modes of the PSS 10 wt % PWA composite material, respectively. Although the BF-STEM image shows a flat surface, the HAADF-STEM image indicates particles of ca. 2.5 nm in diameter with the high contrast. These STEM images were obtained from all of the parts. Since the HAADF-STEM images directly depend on the atomic number,[18] the white contrast is based on the position of the tungsten atom, which was the component substance of the PWA molecule. These results suggest that the PWA-PSS composite material is isotropic and the PWA molecules have been homogeneously nanodispersed in the PSS matrix. Parts a and b of Figure 8 show the ^{31}P MAS NMR and ^{1}H MAS NMR spectra of the PWA-PSS composite material for the various PWA doping ratios, respectively. The ^{31}P NMR spectrum of PWA·29H_2O showed one peak at −15.0 ppm, related to the hydrated PWA molecule.[19] This peak is sensitive for the hydration number of the PWA molecule and known to show a low-field shift from −15 ppm to −11 ppm by the loss of hydrogen bonding with the water molecules.[19] Surprisingly, by mixing of the PSS molecule, this peak shifted about 1.5 ppm (see the (3) spectrum of Figure 8a). These low-field shifts have not been reported and the value of the lowest shift, as far as we know, is −8 ppm for the PWA−zirconia composite material.[20] However, for the high mixing ratio of PWA (%), the main peak of the ^{31}P NMR spectrum appeared again at −15.0 ppm (see the (4) spectrum of Figure 8a). These results suggest that, for the mixing ratio of 10 wt % PWA, the electron density of the P atom decreased mostly due to the interaction with the −SO_3H in PSS through hydrogen bonding. In contrast, the ^{1}H NMR spectrum in the PWA molecule has been known to appear at 9.1 ppm.[20] However, for the PSS-PWA composite material, the ^{1}H NMR spectra did not show the signal at 9.1 ppm. These results suggest that the proton of PWA does not exist on the PWA surface and the free proton interacts with −SO_3H in the PSS molecule. Additionally, the proton of −SO_3H in PSS at 10.76 ppm shifted to 11.14 ppm by mixing with the PWA molecule. This is due to the decrease of the electron density of the proton in −SO_3H. Namely, the proton of −SO_3H has been slightly attracted to the PWA surface by the strong acidity of the PWA molecule.

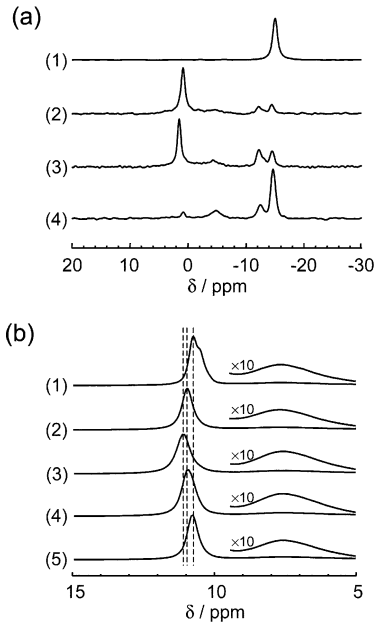

Figure 8. (a) ^{31}P MAS NMR spectra of PWA-PSS composite materials. (1) Pure PWA; (2) PSS 5 wt % PWA; (3) PSS 10 wt % PWA; (4) PSS 50 wt % PWA. (b) ^{1}H MAS NMR spectra of PWA-PSS composite materials. (1) Pure PSS (dried at 70 °C); (2) pure PSS (dried at 150 °C); (3) PSS 5 wt % PWA; (4) PSS 10 wt % PWA; (5) PSS 50 wt % PWA.

Here, we propose a novel anhydrous proton-conducting structure and mechanism. Since the acidity of the molecule is based on the pK_a value, in our research, the PWA and PSS molecules are a Brønsted acid and base, respectively. Therefore, the proton of PWA jumps to −SO_3H in PSS and the proton defect site was constructed on the PWA surface; as a result, the free proton from the PWA molecule interacts with the −SO_3H and forms the protonated −SO_3H, such as −$SO_3H_2^+$. Additionally, the proton of −SO_3H in the PSS molecule was slightly attracted to the PWA surface to compensate for the proton defect of PWA. Furthermore, since the −SO_3H group has been fixed in the backbone of PSS chain, it constructs the closest packing structure on PWA surface. Therefore, we proposed the PWA-encapsulated material, such as Figure 9a. The Keggin-type PWA molecule is more closer to a spherical molecules, and if the encapsulated structure has been hypothesized, the number of −SO_3H groups that cover the PWA surface with the closest packing geometry can be estimated from the ratio between the surface area of PWA and the area of −SO_3H groups (see Figure S1 in the Supporting Information). According to the closest packed PWA-encapsulation model, the whole surface of PWA molecule has been covered with 115 −SO_3H groups and the size of this encapsulated particle is estimated to be ca. 2.5 nm. Surprisingly, this particle size was consistent with that of the HAADF images (see the Figure 7b). The hypothesized proton conduction in the PWA-encapsulated material is as follows (Figure 9b): the −SO_3H in the PSS molecule accepts the free proton from the PWA molecule and forms the protonated sulfonic acid group, such as −$SO_3H_2^+$. The transport of the proton can occur from the protonated −SO_3H to a nonprotonated −SO_3H. Namely, their protonated and nonprotonated −SO_3H in PSS molecule may act as proton donors and acceptors in the anhydrous proton-transfer reactions. As a result, the fast proton transfer occurs at the PWA surface, such as shown in Figure 9c. If these proton-conducting structures of the PWA-encapsulated material were formed based on the closest packing model of the −SO_3H, the mixing ratio of PWA

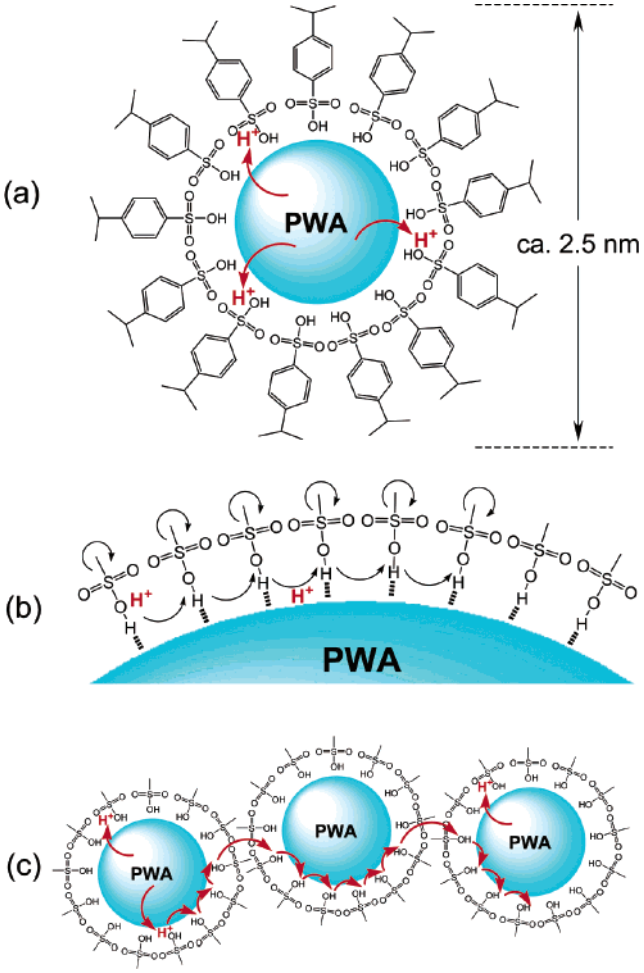

Figure 9. Proposed model of (a) PWA-encapsulated material with the self-assembly of $-SO_3H$ in the PSS molecule. (b) Anhydrous proton-conducting mechanism at the interface between PWA and $-SO_3H$. (c) Proton conduction of nanodispersed PWA-encapsulated material. Arrows indicate the proton transfer or the molecular rotation on the PWA particles in the encapsulated materials. The backbone of PSS chains has been omitted in this model for clarity.

in PSS should be 8.5 wt %, i.e., at PSS 8.5 wt % PWA composite material, all of the surface of PWA has been covered with $-SO_3H$ groups of PSS molecules. Surprisingly again, this value was quite consistent with our experimental value (10 wt %). This maximum anhydrous proton conductivity can be explained as follows (see Figure S2 in the Supporting Information). Basically, the PWA-encapsulated material constructs the fast proton-conducting pathway on the PWA surface, and as a result, the fast proton transfer occurred at the interface between the PWA and $-SO_3H$. Second, under <10 wt % PWA conditions, the proton conductivity decreased due to the existence of interparticle gaps in the PSS molecule. Furthermore, at a > 10 wt % PWA condition, the conductivity decreased again possibly by the reduction of the surface $-SO_3H$ density due to a loss of the self-assembly structure to support the large transport capability of protons

Conclusion

In summary, we proposed a novel fast proton-conducting structure and mechanism. This fast proton transfer under anhydrous conditions has two important points. (1) In the PSS matrix, PWA has been encapsulated by $-SO_3H$, and its $-SO_3H$ has been formed by a self-assembled structure on the PWA surface. (2) The fast anhydrous proton conduction occurs at the interface between PWA and $-SO_3H$. The PWA-encapsulated material may have a potential not only for polymer electrolyte membrane fuel cells operating at intermediate temperatures under anhydrous conditions but also for electrochemical devices including electrochromic displays, chemical sensors, and others.

Acknowledgment. We gratefully acknowledge Dr. Koh-ichi Suzuki and Dr. Shigenobu Hayashi (Research Institute of Instrumentation Frontier, National Institute of Advanced Industrial Science and Technology (AIST)) for the measurements of MAS NMR spectra. This work was supported by R&D program of PEFC by New Energy and Industrial Technology Development Organization (NEDO), Japan.

Supporting Information Available: The calculation of the closest packing model (Figure S1). Change of the anhydrous proton conductivities at 180 °C as a function of PWA mixing ratio (Figure S2). This material is available free of charge via the Internet at http://pubs.acs.org.

References and Notes

(1) (a) Pope, M. T. *Heteropoly and Isopoly Oxometalates*; Springer-Verlag: Berlin, 1983. (b) Drago, R. S.; Dias, J. A.; Maier, T. O. *J. Am. Chem. Soc.* **1997**, *119*, 7702.

(2) Pope, M. T.; Müller, A. *Angew. Chem., Int. Ed. Engl.* **1991**, *30*, 34.

(3) (a) Mizuno, M.; Misono, M. *Chem. Rev.* **1998**, *98*, 199. (b) Okuhara, T. *Chem. Rev.* **2002**, *102*, 3641. (c) Hori, H.; Hayakawa, E.; Einaga, H.; Kutsuna, S.; Koike, K.; Ibusuki, T.; Kiatagawa, H.; Arakawa, R. *Environ. Sci. Technol.* **2004**, *38*, 6118.

(4) Nakamura, O.; Kodama, T.; Ogino, I.; Miyake, Y. *Chem. Lett.* **1979**, 17.

(5) (a) Honma, I.; Takeda, Y.; Bae, J. M. *Solid State Ionics* **1999**, *120*, 255. (b) Honma, I.; Nakajima, H.; Nishikawa, O.; Sugimoto, T.; Nomura, S. *Solid State Ionics* **2003**, *162−163*, 237.

(6) (a) Zaidi, S. M. J.; Mikhailenko, S. D.; Robertson, G. P.; Guiver, M. D.; Kaliaguine, S. *J. Membr. Sci.* 2000, *173*, 17. (b) Tazi, B.; Savadogo, O. *Electrochim. Acta* 2000, *45*, 4329. (c) Malhotra, S.; Datta, R. *J. Electrochem. Soc.* **1997**, *144*, L23.

(7) Colomban, P.; Novak, A. *J. Mol. Struct.* **1988**, *177*, 277.

(8) Kreuer, K. D. *Chem. Mater.* **1996**, *8*, 610.

(9) (a) Hickner, M. A.; Ghassemi, H.; Kim, Y. S.; Einsla, B. R.; McGrath, J. E. *Chem. Rev.* **2004**, *104*, 4587. (b) Li, Q.; He, R.; Jensen, J. O.; Bjerrum, N. J. *Chem. Mater.* **2003**, *15*, 4896. (c) Ma, Y. L.; Wainright, J. S.; Litt, M. H.; Savinell, R. F. *J. Electrochem. Soc.* **2004**, *151*, A8. (d) He, R.; Li, Q.; Xian, G.; Bjerrum, N. J. *J. Membr. Sci.* **2003**, *226*, 169. (e) Rikukawa, M.; Sanui, K. *Prog. Polym. Sci.* **2000**, *25*, 1463.

(10) (a) Kim, Y. S.; Wang, F.; Hickner, M.; Zawodzinski, T. A.; McGrath, J. E. *J. Membr. Sci.* **2003**, *212*, 263. (b) Bordiga, C. P. S.; Zecchina, A. *Langmuir* **2000**, *16*, 8139. (c) Rocchiccioli-Deltcheff, C.; Fournier, M.; Franck, R.; Thouvenot, R. *Inorg. Chem.* **1983**, *22*, 207.

(11) Yamada, M.; Honma, I. *J. Phys. Chem. B* **2004**, *108*, 5522.

(12) Yamada, M.; Honma, I. *Angew. Chem., Int. Ed.* **2004**, *43*, 3688.

(13) Yamada, M.; Honma, I. *Chem. Phys. Chem.* **2004**, *5*, 724.

(14) Sone, Y.; Ekdunge, P.; Simonsson, D. *J. Electrochem. Soc.* **1996**, *143*, 1254.

(15) Iwahara, H. *Solid State Ionics* **1996**, *86−88*, 9.

(16) Li, Y. M.; Hibino, M.; Miyayania, M.; Kudo, T. *Solid State Ionics* **2000**, *134*, 271.

(17) (a) Hinokuma, K.; Ata, M. *Chem. Phys. Lett.* **2001**, *341*, 442. (b) Hinokuma, K.; Ata, M. *J. Electrochem. Soc.* **2003**, *150*, A112.

(18) Pennycook, S. J.; Jesoon, D. E. *Phys. Rev. Lett.* **1990**, *64*, 938.

(19) (a) Uchida, S.; Inumaru, K.; Misono, M. *J. Phys. Chem. B* **2000**, *104*, 8108. (b) Ueda, T.; Tatsumi, T.; Eguchi, T.; Nakamura, N. *J. Phys. Chem. B* **2001**, *105*, 5391.

(20) López-Salinas, E.; Hernández-Cortéz, J. G.; Schifter, I.; Torres-García, E.; Navarrete, J.; Gutiérrez-Carrillo, A.; López, T.; Lottici, P. P.; Bersani, D. *Appl. Catal. A* **2000**, *193*, 215.